DE GRUYTER OPEN

Journal of ELECTRICAL ENGINEERING, VOL 67 (2016), NO5, 334–342

A NEW HIGH SPEED INDUCTION MOTOR DRIVE BASED ON FIELD ORIENTATION AND HYSTERESIS CURRENT COMPARISON

Cosmas Ogbuka — Cajethan Nwosu — Marcel Agu *

This paper presents a new high speed induction motor drive based on the core advantage of field orientation control (FOC) and hysteresis current comparison (HCC). A complete closed loop speed-controlled induction motor drive system is developed consisting of an outer speed and an inner HCC algorithm which are optimised to obtain fast and stable speed response with effective current and torque tracking, both during transient and steady states. The developed model, being speed-controlled, was examined with step and ramp speed references and excellent performances obtained under full load stress. A speed response comparison of the model with the standard AC3 (Field-Oriented Control Induction Motor Drive) of MATLAB Simpower systems shows that the model achieved a rise time of 0.0762 seconds compared to 0.2930 seconds achieved by the AC3. Also, a settle time of 0.0775 seconds was obtained with the developed model while that of the AC3 model is 0.2986 seconds confirming, therefore, the superiority of the developed model over the AC3 model which, hitherto, served as a reference standard.

K e y w o r d s: induction motor drive, hysteresis current control, field orientation, vector control

1 INTRODUCTION

The induction motor (IM), particularly, the squirrel-cage type, is widely used in electric drives and is responsible for most of the energy consumed by electric motors [1], hence it is called the workhorse of the industry [2–6] because it has mechanical ruggedness, high robustness, design simplicity, reliability, economy, control flexibility, less maintenance requirement, generally satisfactory efficiency and ability to operate in explosive and corrosive environments compared to other machines in ac drives [3,4, 7–9].

The dominance of induction motors in industry has continued despite the emergence of new motor types such as the permanent magnet synchronous motors which share some merits as well as some far-reaching limitations [10–12]. Clearly, the induction motors will dominate in industrial drives for decades and this is the fact behind the sustained research efforts, particularly, in energy-efficient adjustable speed drives (ASD) [13–15]. ASD becomes very pertinent because induction motors do not have constant speed characteristics during load changes and are, inherently, not capable of variable speed operation. Recent developments in the theory of vector control, fast digital processor and power electronic devices provide the possibility of achieving high performance induction motor drive control [17].

Since torque is proportional to current either in the stationary or rotor reference frames and control of current gives control of torque and speed, current control strategies are employed in ASD to ensure that stator currents track their respective reference values. Prominent among the current control strategies is the Hysteresis Current Control (HCC) due to ease of implementation, excellent transient response, attainment of maximum current limit and insensitive to load parameter variations [11, 18–22].

In this work, a high speed induction motor drive based on the core advantage of field orientation control (FOC) and hysteresis current control was developed. The control parameters were optimised to obtain fast speed response and effective tracking of current and torque. The system being a speed-controlled drive, the performance of the developed model was examined with step and ramp speed input under full load stress to examine the transient and steady state performance. Finally, the developed model is compared with the AC3 model (Field-Oriented Control Induction Motor Drive) of MATLAB Simpower System in terms of response speed.

2 INDUCTION MOTOR MODEL AND FIELD ORIENTATION CONTROL (FOC)

Recall the dynamic voltage equations of the squirrel cage induction motor in the synchronously rotating reference frame, the electromagnetic torque equation and the rotor dynamic equation as shown from the following equations [23, 24].

$$\begin{bmatrix} v_{ds} & v_{qs} & 0 & 0 \end{bmatrix}^\top = \begin{bmatrix} R_s + pL_s & -\omega_e L_s & pL_m & -\omega_e L_m \\ \omega_e L_s & R_s + pL_s & \omega_e L_m & pL_m \\ pL_m & -\omega_{sl} L_m & R_r + pL_r & -\omega_{sl} L_r \\ \omega_{sl} L_m & pL_m & \omega_{sl} L_r & R_r + pL_r \end{bmatrix} \begin{bmatrix} i_{ds} \\ i_{qs} \\ i_{dr} \\ i_{qr} \end{bmatrix}, \quad (1)$$

* Department of Electrical Engineering, University of Nigeria, Nsukka, Nigeria
cosmas.ogbuka@unn.edu.ng, cajethan.nwosu@unn.edu.ng, marcel.agu@unn.edu.ng

DOI: 10.1515/jee-2016-0048, Print (till 2015) ISSN 1335-3632, On-line ISSN 1339-309X

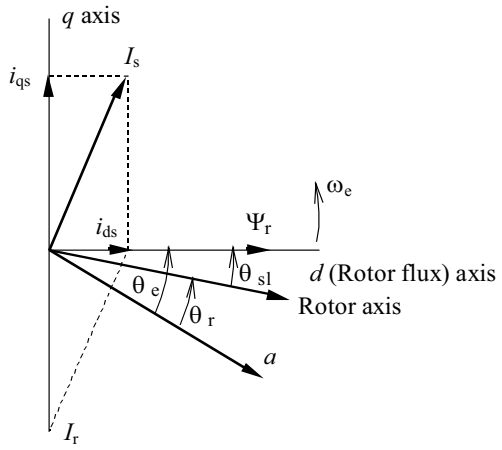

Fig. 1. Phasor diagram of FOC for induction motor

$$T_e = \frac{3}{2}\frac{P}{2}\frac{L_m}{L_r}\left(\psi_{dr} i_{qs} - \psi_{qr} i_{ds}\right), \tag{2}$$

$$T_e = T_L + B\omega_r + Jp\omega_r\,, \tag{3}$$

where $v_{ds}, v_{qs} = d, q$-axis stator voltages; $R_s, R_r =$stator, rotor resistances; $L_s, L_r, L_m =$stator, rotor, magnetizing inductances; $L_{lr}, L_{ls} =$rotor, stator leakage inductances; $L_r = L_{lr} + L_m$; $L_s = L_{ls} + L_m$; $\omega_r, \omega_e, \omega_{sl} =$rotor, synchronous, slip speeds; $P =$number of poles; $\omega_{sl} = \omega_e - \frac{P}{2}\omega_r$; $\psi_{dr}, \psi_{qr} = d, q$-axis rotor flux linkages; $p =$differential operator; $T_e =$electromagnetic torque; $T_L =$load torque; $B =$rotor damping coefficient; $J =$inertia constant.

The FOC controls the stator current vector of the induction machine to achieve a precise and independent control of torque and flux as obtainable in the dc machines. The stator current vector contains the torque controlling component, i_{qs}, and the flux controlling component, i_{ds} as shown in the phasor diagram of Fig. 1.

From Fig. 1, field orientation is feasible because the entire rotor flux ψ_r is aligned to the d-axis thereby making the q-axis flux component ψ_{qr} zero since they are perpendicular to each other. Consequently, (2) reduces to (4) where $T_e \propto i_{qs}$. Also, from the rotor flux orientation described above, equation (5) shows that the rotor flux $\psi_r \propto i_{ds}$.

$$T_e = \frac{3}{2}\frac{P}{2}\frac{L_m}{L_r}\psi_{dr} i_{qs}\,, \tag{4}$$

$$\psi_r = \psi_{dr} = L_m i_{ds}\,. \tag{5}$$

Under this condition, the induction motor behaves exactly as the separately excited dc motor where the q-axis stator current i_{qs} entirely controls the electromagnetic torque and the d-axis stator current i_{ds} entirely controls rotor flux.

3 OVERALL SCHEMATIC OF THE DRIVE SYSTEM

The induction motor in the scheme of Fig. 2 is fed by a hysteresis current-controlled PWM inverter operating as a three-phase sinusoidal current source. The power

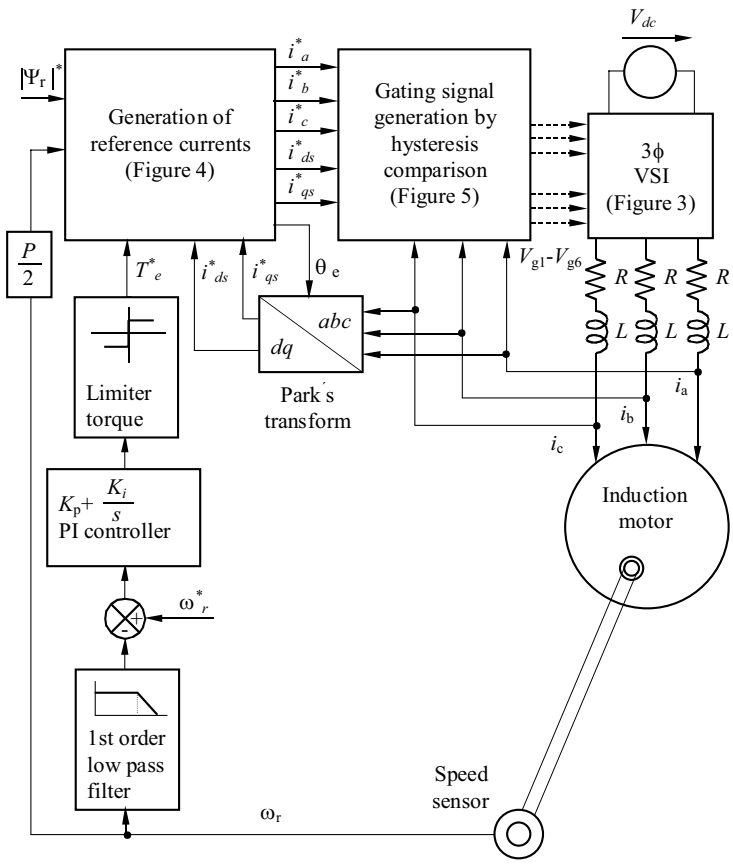

Fig. 2. Complete schematic of the speed-controlled induction motor drive system

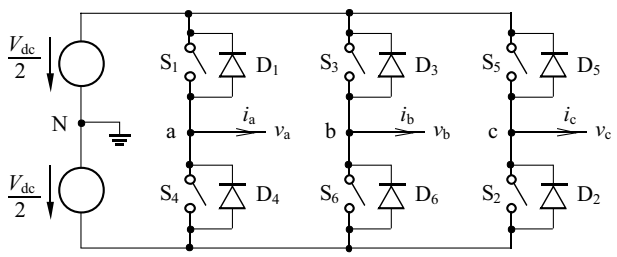

Fig. 3. Power circuit of three-phase inverter

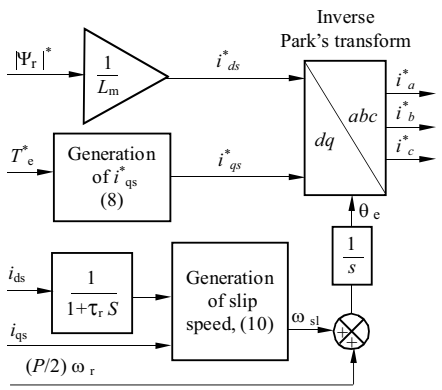

Fig. 4. Generation of reference phase currents

circuit of the inverter is shown in Fig. 3. The rotor speed ω_r is sensed by the speed sensor and filtered by the 1st order low pass filter. The speed error between the actual rotor speed and its reference is processed through the proportional-integral (PI) speed controller to nullify the steady state error in speed. The output is restricted to an upper and a lower limit to produce a realistic reference torque T_e^*. Figure 4 shows the realisation of the reference phase currents as expressed from equation (6) to (13). All reference or command values are superscripted with * in the diagrams.

$$i^*_{ds} = \frac{|\psi_r|^*}{L_m}\,, \tag{6}$$

$$\psi_r = \frac{L_m i_{ds}}{1+\tau_r s} \tag{7}$$

where $\tau_r = L_r/R_r$ is the rotor time constant.

$$i^*_{qs} = \frac{2}{3}\frac{2}{P}\frac{L_r}{L_m}\frac{T^*_e}{\psi_r}\,, \tag{8}$$

$$i^*_s = \sqrt{i^*_{ds} + i^*_{qs}}\,, \tag{9}$$

$$\omega_{sl} = \frac{L_m}{\psi_r}\frac{R_r}{L_r} i_{qs}\,, \tag{10}$$

$$\theta_e = \int \Big(\frac{P}{2}\omega_r + \omega_{sl}\Big)\mathrm{d}t\,, \tag{11}$$

$$\begin{aligned} i_{qs} &= \tfrac{2}{3}\big(i_a\cos\theta_e + i_b\cos\big(\theta_e - \tfrac{2\pi}{3}\big) + i_c\cos\big(\theta_e + \tfrac{2\pi}{3}\big)\big),\\ i_{ds} &= \tfrac{2}{3}\big(i_a\sin\theta_e + i_b\sin\big(\theta_e - \tfrac{2\pi}{3}\big) + i_c\sin\big(\theta_e + \tfrac{2\pi}{3}\big)\big). \end{aligned} \tag{12}$$

The reference phase currents are computed using the inverse park's transform as

$$\begin{aligned} i^*_a &= i^*_{qs}\cos\theta_e + i^*_{ds}\sin\theta_e\,,\\ i^*_b &= i^*_{qs}\cos\big(\theta_e - \tfrac{2\pi}{3}\big) + i^*_{ds}\sin\big(\theta_e - \tfrac{2\pi}{3}\big)\,,\\ i^*_c &= i^*_{qs}\cos\big(\theta_e + \tfrac{2\pi}{3}\big) + i^*_{ds}\sin\big(\theta_e + \tfrac{2\pi}{3}\big)\,. \end{aligned} \tag{13}$$

The reference phase currents (i^*_a, i^*_b and i^*_c) and the actual phase currents (i_a, i_b and i_c) are compared, by feedback. Error signals are generated and used in the control logic of appendix one to generate the voltage gating signals for the switches of the three phase inverter. The HCC action is made possible by Δi^*_s where Δ is an adjustable hysteresis window which determines the effectiveness of current and torque tracking.

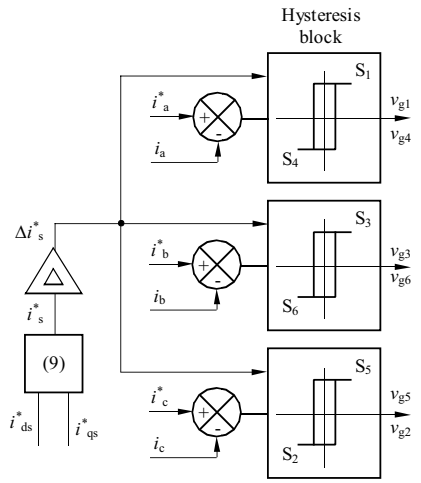

Fig. 5. Generation of inverter voltage gating signals

Current control is achieved as illustrated in Fig. 5 by the appropriate firing of the power semiconductor switches S_1 to S_6 of the three phase inverter. The inverter is supplied by an adequately filtered dc source V_{dc}. Each phase current to the motor is limited by the series RL branch ($R = 0.001\,\Omega$ and $L = 5$ mH).

4 RESULTS AND DISCUSSIONS

The complete drive system is simulated for the motor of appendix two and the results presented under three headings (i) Hysteresis comparison a pulse width modulation, (ii) Response to step speed input, (iii) Response to ramp speed input. To obtain the best possible performance, tuning method was employed to obtain the optimal proportional and integral gain values. It is an industrial practice to lower the proportional and integral gain values and gradually tune them up until the best possible performance is achieved. This is procedure is adopted here.. The optimal control variables are: Proportional gain $= 5$, Integral gain $= 100$, 1st order low pass filter time constant $= 1.6 \times 10^{-3}$ seconds, Torque limiter upper lower $= 75$ Nm/-75 Nm.

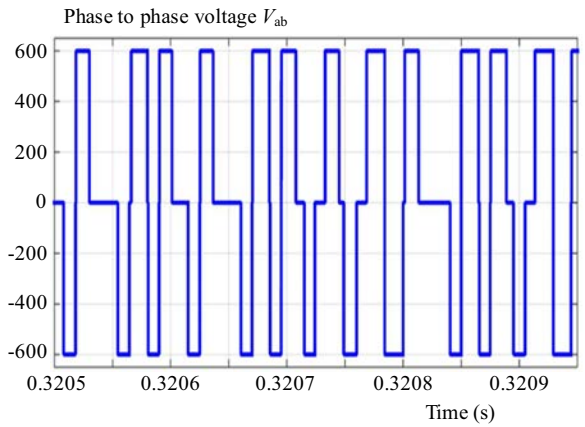

Fig. 6. Phase to phase voltage v_{ab}

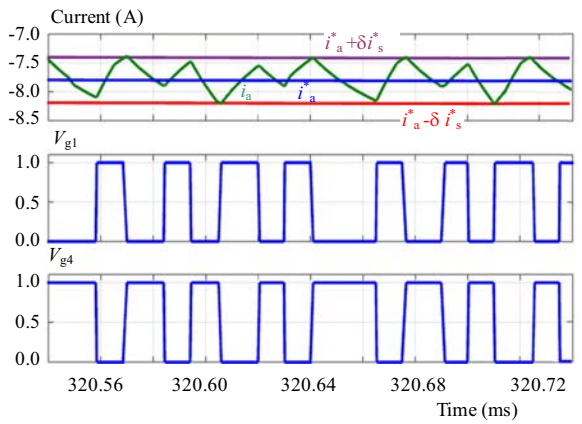

Fig. 7. Hysteresis current and gating signals at $\Delta = 0.05$

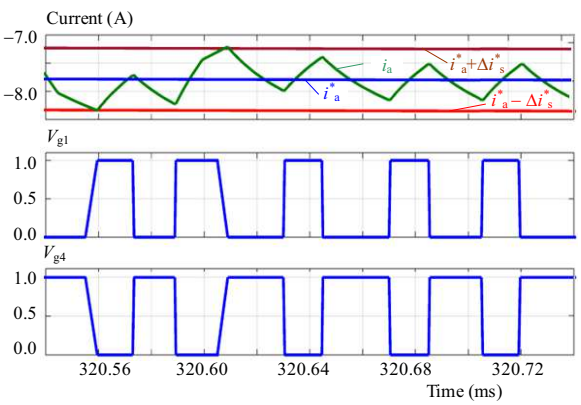

Fig. 8. Hysteresis current and gating signals at $\Delta = 0.07$

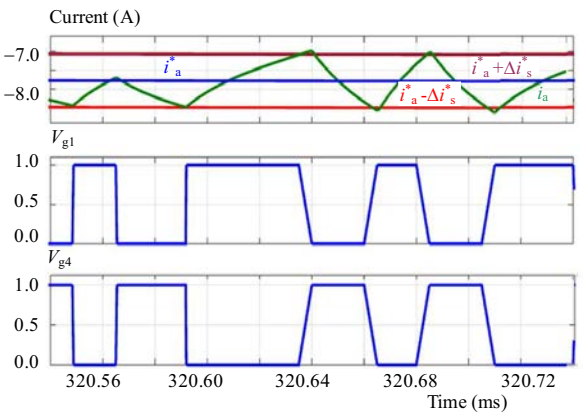

Fig. 9. Hysteresis current and gating signals at $\Delta = 0.09$

4.1 Hysteresis Comparison as Pulse Width Modulation

The no load run of the motor at a constant speed of 500 rpm is used to illustrate the hysteresis comparison as pulse width modulation. Figure 6 shows the inverter phase to phase voltage v_{ab}. Similar results are obtained for v_{bc} and v_{ca}. The variation and delay in the conduction time of the inverter switches highlights the pulsewidth modulation nature of the hysteresis current comparison.

For the narrow time range of 0.3205 to 0.3207, the voltage gating signals, vg1 and vg4, for the complementary switches in the first leg of the inverter, S_1 and S_4, are shown in Fig. 7 for hysteresis band $\Delta = 0.05$ using phase 'a' to highlight the hysteresis property for purpose of clarity. It can be seen that the two switches conduct alternately as earlier explained. The phase 'a' current i_a tracts the upper boundary $i^*_a + \Delta i^*_s$ (increases) when switch S_1 is conducting and tracts the lower boundary $i^*_a - \Delta i^*_s$ (decreases) when switch S_4 is conducting. The hysteresis current control action, which makes i_a to track its reference i^*_a, is seen as i_a moves between $i^*_a + \Delta i^*_s$ to $i^*_a - \Delta i^*_s$ as switches S_1 and S_4 conduct alternately. Still using the 'a' phase, the procedure is repeated for $\Delta = 0.07$ and 0.09 as shown in Figs. 8 and 9 respectively. It can be seen from the pulse widths that the switching speed decreases as the hysteresis band is increased. As a result, the best i_a tracking of i^*_a is when the hysteresis band is narrowest ($ie\,\Delta = 0.05$). Smaller hysteresis bands imply higher switching frequency. This may constitute a practical limitation on the power device switching capability due to switching losses which need to be mitigated.

Figures 10–12 show the hysteresis current control property for the phases a, b and c respectively for the same narrow time band. Phase shift of 120 degrees between the phases is observed.

4.2 Response to Step Speed Input (1000 rpm to 500 rpm to −500 rpm)

The motor is started at a reference speed input of 1000 rpm at no load as shown in Figs. 13 and 14. At 0.4 seconds, the speed reference is stepped-down to 500 rpm with a simultaneous application of 49.9 Nm rated load. At 0.8 4seconds, a negative speed command of −500 rpm is applied with the load torque removed.

As shown in Fig. 14, to sustain speed rise during starting from rest, the electromagnetic torque rises even at no load. The motor briefly enters into generation mode as soon as the speed crosses the reference. This forces the reference and the electromagnetic torque to negative before stabilising at zero during steady state since no load is applied.

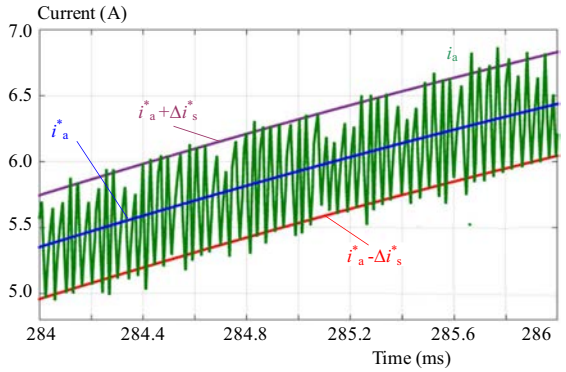

Fig. 10. Hysteresis current tracking for phase 'a'

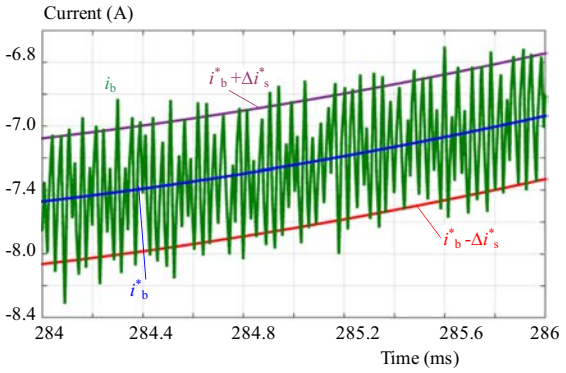

Fig. 11. Hysteresis current tracking for phase 'b'

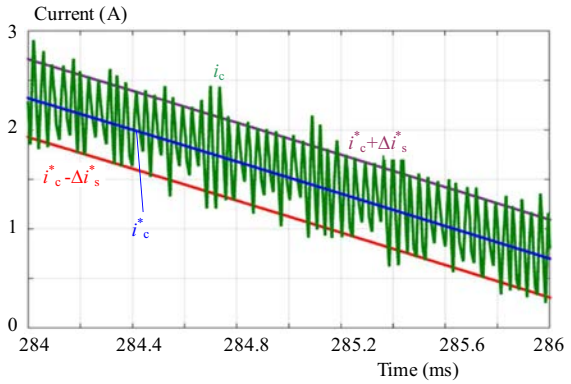

Fig. 12. Hysteresis current tracking for phase 'c'

Simultaneous application of rated load (49.9 Nm) and step-down of speed to 500 rpm at 0.4 seconds forces the reference and electromagnetic toques to the negative extreme (−75 Nm). This enables speed decrease. The electromagnetic toque is less than the reference due to the frictional effect of the load.

When the speed crosses the reference, the electromagnetic and the reference torque instantly rises above the load torque to support regeneration before the electromagnetic torque settles to the load torque at steady state. The reference toque remains above that the load torque by a proportion of the frictional effect of the load.

Negative step speed command of −500 rpm and load removal is made at 0.8 seconds resulting, instantly, on the reference and electromagnetic torque of −75 Nm since load is zero. Electromagnetic torque, thereafter, decreases with speed until speed crosses the reference. After the brief period of regeneration, the reference and the electromagnetic torque settles at zero since load is zero.

Figures 15 and 16, respectively, show the reference stator phase and the actual stator phase currents. The phase currents responded to the speed and load changes. The actual phase current effectively tracks the reference values.

The switching speed decreased by 100 % when speed is changed from 1000 rpm to 500 rpm as shown, more clearly, for 'a' phase in Fig. 17. The switching speed is the same both for 500 rpm and −500 rpm. An expanded view, Fig. 18, is shown of the nature of the phase current inversion (reversal) from a-b-c to c-b-a at the instant of speed change from 500 rpm to −500 rpm (positive to negative).

Rotor position which is zero at start, as seen in Fig. 19, increases for as long as speed remains positive but creates a new orientation at each instant of speed change but reverses direction with speed reversal.

4.3 Response to ramp speed input (500 rpm to −500 rpm to 500 rpm)

The interest here is to observe the motor behaviour during negative and positive ramp speed commands under simultaneous full load stress.

Negative ramp speed command of −500 rpm is made from 0.3 seconds to 0.6 seconds at full load stress as shown in Figs. 20 and 21. The load is removed at

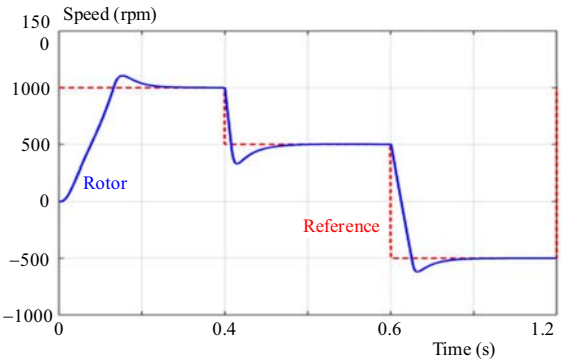

Fig. 13. Reference and rotor speed for step speed input

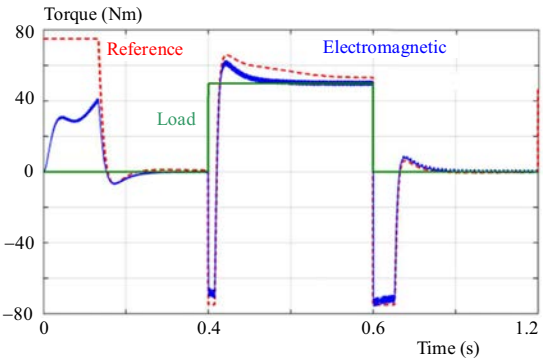

Fig. 14. T_{ref} , T_e , and T_L for step speed input

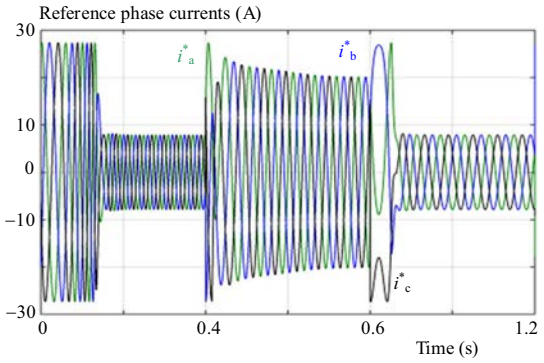

Fig. 15. Reference phase currents for step speed input

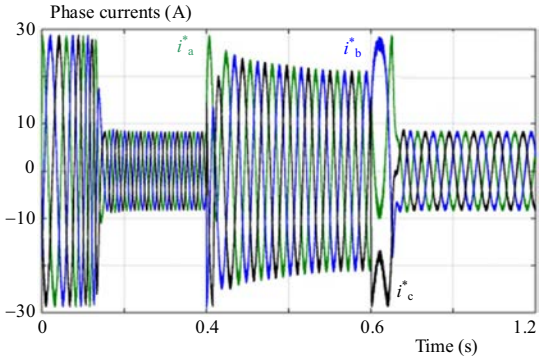

Fig. 16. Actual phase currents for step speed input

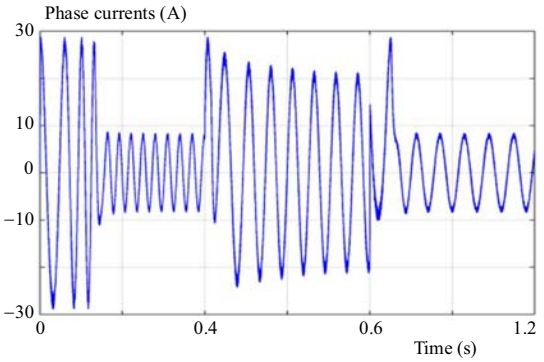

Fig. 17. Phase – a current

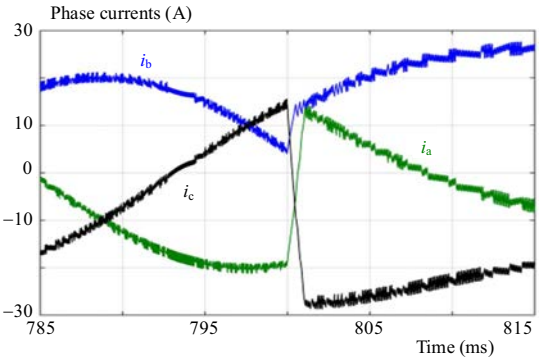

Fig. 18. Phase current reversal for step speed input (expanded)

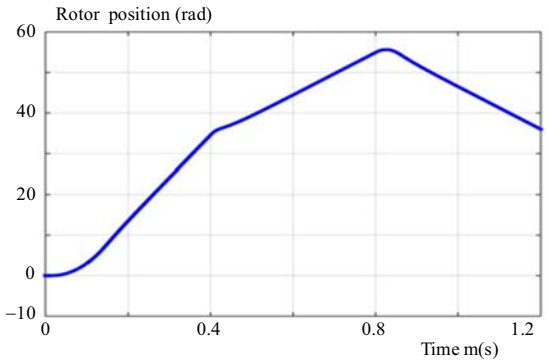

Fig. 19. Rotor position θ_r for step speed input

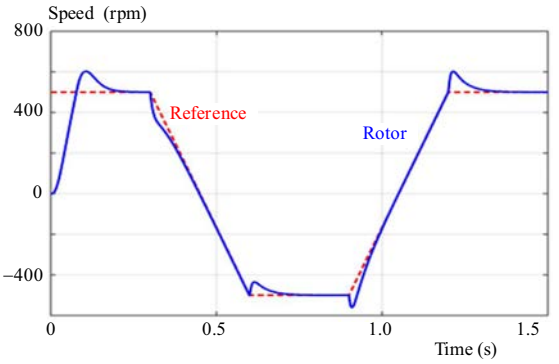

Fig. 20. Reference and actual rotor speed for RAMP speed input

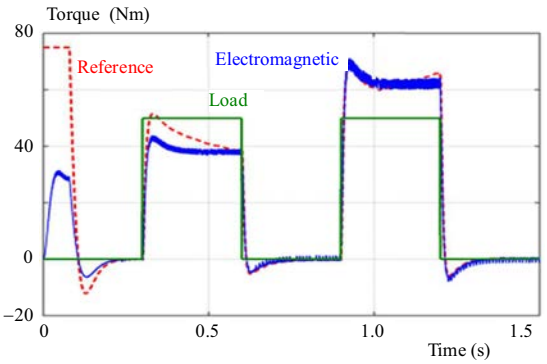

Fig. 21. T_{ref} , T_e and T_L for RAMP speed input

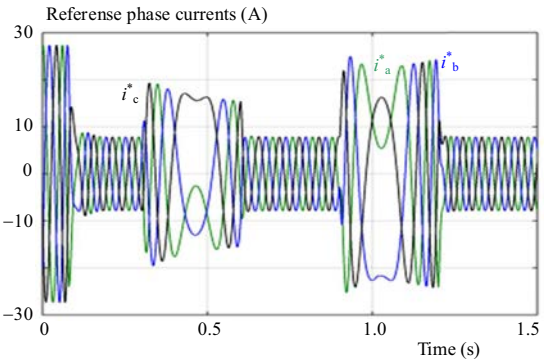

Fig. 22. Reference phase currents for RAMP speed input

0.6 seconds when −500 rpm is attained. Between 0.9 seconds and 1.2 seconds, a positive ramp speed command is made on full load. As can be seen, ramping provides a gradual speed transition thereby enabling the actual rotor speed to trace the path of the reference speed input very closely. The effect of gain and loss of load at the inception and end of ramping respectively can be seen of the rotor speed. The frictional effect of the load torque as well as the torque gradient due to the gradual speed change during ramping are also observed.

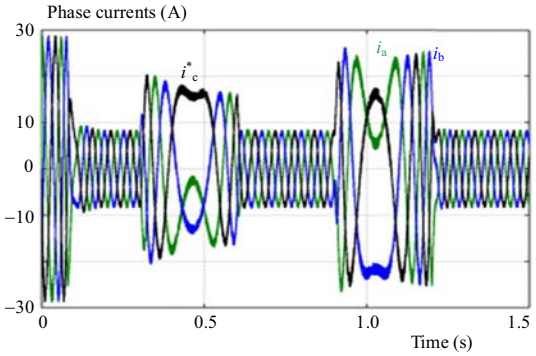

Fig. 23. Actual phase currents for RAMP speed input

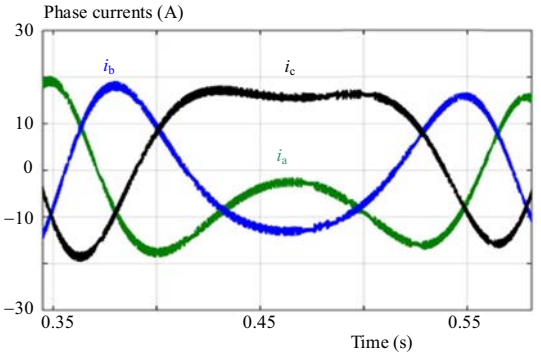

Fig. 24. Phase current reversal for RAMP speed input (expanded)

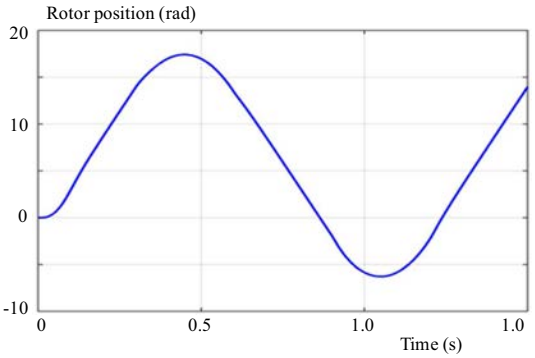

Fig. 25. Rotor position θ_r for step speed input

The speed ramps occurred simultaneously at rated loading of 49.9 Nm as shown in Fig. 21. Unlike in the step input where the reference torque takes its minimum value at the instant of speed reversal thereby, momentarily, forcing the electromagnetic torque to the negative extreme, the torque profile during speed ramping from positive to negative is positive due to the gradual speed transition. At steady state, the electromagnetic torque and the reference torque are zero since no loading occurred during steady state.

Phase current sequence reversal also occur at the two instances of speed change from positive to negative just as in the case of step speed input, as seen in Figs. 22–24. A comparison of Figs. 18 and 24, however, show that ramp speed command provides a smooth speed transition offering excellent dynamic stability during phase reversal. The rotor position shown in Fig. 25 smoothly changes orientation at each instant of speed reversal.

5 DRIVE COMPARISON WITH AC3 OF MATLAB SIMPOWER SYSTEM

The dynamic speed response of the developed model is compared with the standard AC3 of MATLAB simpower system under exactly the same control condition of the same 10 Hp induction motor for a constant speed command of 500 rpm on no load. Emphasis is on the rise and settling time of the speed response for the two models.

With rise time defined as the time to attains 98 % of the final value (98 % of 500 rpm is 490 rpm), the rise time for our developed model is 0.0762 seconds while the rise time for AC3 model is 0.2930 seconds as shown in Fig. 26(a) and (b) respectively.

The two systems are critically damped; meaning that the settle time coincidence with the final value time. The settle time for our developed model is 0.0775 seconds while that of the AC3 model is 0.2986 seconds as shown in Fig. 26(c) and (d) respectively.

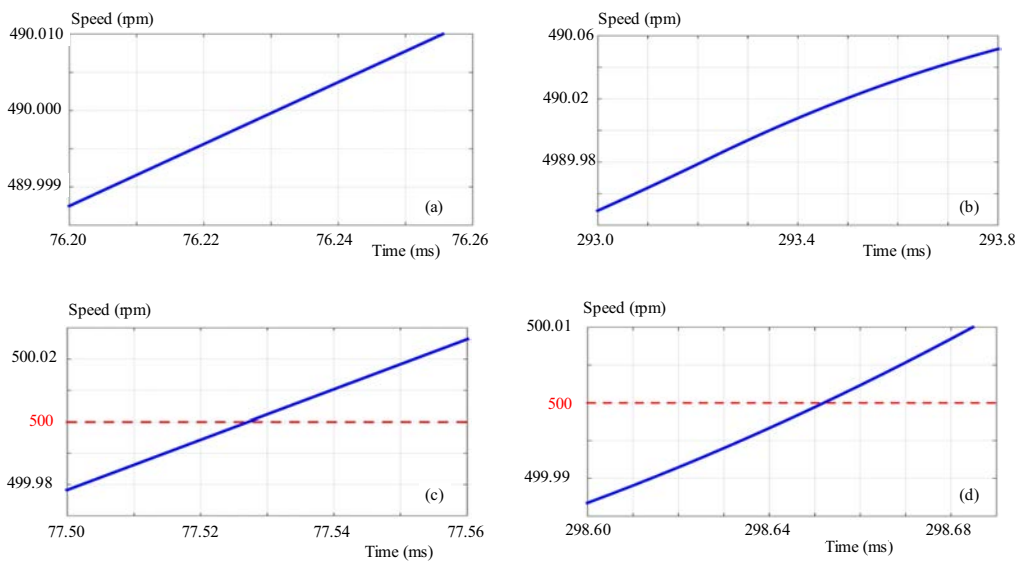

Fig. 26. Rise and settle time for the deveq loped (a), (c) and AC3 models (b), (d) respectivelly

6 CONCLUSION

This work has presented a new high speed induction motor drive based on field orientation and hysteresis current comparison. The results show that the set objectives of the research have been achieved.

Since torque can be made proportional to current either in the stationary or rotor reference frames and effective control of current gives effective control of torque, current control by hysteresis comparison has been utilised to drive a three phase inverter controlling a three induction motor whose stator current has been decoupled just as in DC motors to achieve independent and precise control of torque and flux.

The developed speed-controlled drive consisting of an outer PI speed controller and an inner HCC current controller was optimised to yield fast speed response under full load stress for step and ramp speed inputs. In each, the HCC strategy has been used to ensure that the actual motor phase currents tracked their respective sinusoidal references. Gradual speed transition due to speed reversal was obtained during speed ramping thereby permitting the speed profile to remain positive all through unlike in the speed input which forced the torque reference to the negative limit at the instant of speed reversal.

When compared to the standard AC3 of MATLAB Simpower systems which attained a rise time of 0.2930 seconds, a rise time of 0.0762 seconds was attained by the developed model. Similarly, the settle time of the AC3 is 0.2986 while that of the developed model is 0.0775. Clearly, the developed model has shown superiority over the AC3 model which, hitherto, served as a reference standard.

Appendix 1: Inverter switch gating voltage signal estimation

(a) For inverter phase "a" leg

If $i_a < i_a^* - \Delta i_s^*$ OR $(i_a > i_a^* - \Delta i_s^*$ AND $i_a < i_a^* + \Delta i_s^*$ AND $\frac{\mathrm{d}i_a}{\mathrm{d}t} > 0)$

$v_{g1} = 1;\ v_{g4} = 0$

else $v_{g1} = 0;\ v_{g4} = 1$

end

(b) For inverter phase "b" leg

If $i_b < i_b^* - \Delta i_s^*$ OR $(i_b > i_b^* - \Delta i_s^*$ AND $i_b < i_b^* + \Delta i_s^*$ AND $\frac{\mathrm{d}i_b}{\mathrm{d}t} > 0)$

$v_{g3} = 1;\ v_{g6} = 0$

else $v_{g3} = 0;\ v_{g6} = 1$

end

(c) For inverter phase "c" leg

If $i_c < i_c^* - \Delta i_s^*$ OR $(i_c > i_c^* - \Delta i_s^*$ AND $i_c < i_c^* + \Delta i_s^*$ AND $\frac{\mathrm{d}i_c}{\mathrm{d}t} > 0)$

$v_{g5} = 1;\ v_{g2} = 0$

else $v_{g5} = 0;\ v_{g2} = 1$

end

Appendix 2: Sample squirrel cage induction motors

Rated Power, Hp	10
Rated Line Voltage, V	400
Rated Frequency, Hz	50
Stator Resistance, Ω	0.7384
Stator leakage inductance, H	0.003045
Rotor Resistance Referred to Stator, Ω	0.7402
Rotor Leakage Inductance Referred to the Stator, H	0.003045
Mutual Inductance, H	0.1241
No. of Poles	4
Motor Inertia, Kgm^2	0.0342
Motor Friction Factor	0.000503
Direct Axis Rotor Flux, wb/sec	0.97644
Speed, rpm	1440
Rate Torque, Nm	49.9

References

[1] GARCIA, G.—LUIS, J.—STEPHAN, R.—WATANABE, E.: An Efficient Controller for an Adjustable Speed Induction Motor Drive, IEEE Trans. on Industrial Electronics **41** No. 5 (Oct 1994), 533–539.

[2] KORLINCHAK, C. Comanescu,—M.: Sensorless Field Orientation of an Induction Motor Drive using a Time-Varying Observer, IET Electric Power Application **6** No. 6 (2012), 353–361.

[3] UDDIN, M. Wen—H.: Development of a Self-Tuned Neuro-Fuzzy Controller for Induction Motor Drives, IEEE Trans. on Industry Applications **43** No. 4 (July/Aug 2007), 1108–1116.

[4] BOSE, B. K.: Power Electronics and Motion Control-Technology Status and Recent Trends, IEEE Trans. on Industry Applications **29** No. 5 (Sep/Oct 1993), 902–909.

[5] TOLIYAT, H.—XU, L.—LIPO, T. A.: A Five-Phase Reluctance Motor with High Specific Torque, IEEE Trans. on Industry Applications 28 No. 3 (May/June 1992), 659–667.

[6] BÖCKER, J.: State of the Art of Induction Motor Control, IEEE International Conference on Electric machines and Drives, Antalya, May 2007, pp. 1459–1464.

[7] DAS, S.—PAL, A.—KUMAR, R.—CHATTOPADHYAY, A. K.: An Improved Rotor Flux Based Model Reference Adaptive Controller for Four-Quadrant Vector Controlled Induction Motor Drives, IEEE Region 10 Conference (TENCON2015), Macao, Nov 2015, pp. 1–6.

[8] PETER, J.—MARQUES, G. D.—RAMCHAND, R.: Current Error Space Vector Based Constant Switching Frequency Hysteresis Controller for VSI Fed Induction Motor Drives, IEEE 9th International conference on Compatibility and power electronics (CPE), Costa da Caparica, June 2015, pp. 246–251.

[9] HUANG, C. Y.—WEI, C. P.—YU, J. T—HU, Y. J.: Torque and Current Control of Induction Motor Drives for Inverter Switching Frequency Reduction, IEEE Trans. on Industrial Electronics **52** No. 5 (Oct 2005), 1364–1371.

[10] PILLAY, P.—KRISHNANR.: Modeling, Simulation, and Analysis of Permanent Magnet Motor Drives I: The Permanent Magnet Synchronous Motor Drive, IEEE Trans. on Industrial Application **25** No. 2 (1989), 265–273.

[11] OGBUKA, C.—NWOSU, C.—AGU, M.: A Fast Hysteresis Current-Controlled Permanent Magnet Synchronous Drive Based on Field Orientation Journal of Electrical Engineering (Elektrotechnicky Casopis).

[12] MORIMOTO, S.—OOI, S.—INOUE, Y.—SANADA, M.: Experimental Evaluation of a Rare-Earth-Free Pmasynrm with Ferrite Magnets for Automotive Applications, IEEE Trans. on Industrial Electronic **61** No. 10 ((Jan 2014), 5749–5756.

[13] FARASAT, M.—TRZYNADLOWSKI, A. M.—FADALI, M. S.: Efficiency Improved Sensorless Control Scheme for Electric Vehicle Induction Motors, IET Electrical Systems in Transportation **4** No. 4 (2014), 122–131.

[14] SUNG, W.—SHIN, J.—JEONG, Y.: Energy-Efficient and Robust Control for High-Performance Induction Motor Drive with an Application in Electric Vehicles, IEEE Trans. on Vehicular Technology **61** No. 8 (Oct 2012), 3394–3405.

[15] JAHMEERBACUS, M. I.: Flux Vector Control of an Induction Motor Drive for Energy-Efficient Operation of a Centrifugal Pump, Proceedings of the IEEE International Conference on Industrial Engineering and Operations Management, Dubai, United Arab Emirates (UAE), 2015, pp. 1–6.

[16] KUMAR, B.—CHAUHAN, Y. K.—SHRIVASTAVA, V.: Investigations on Energy Efficient Sensorless Induction Motor Drive, International Conference on Computing, Communication and Automation (ICCCA2015), Noida, May 2015, pp. 974–978.

[17] El-KHOLY, E.: A High Performance Induction Motor Drive Based on Adaptive Variable Structure Control, Journal of Electrical Engineering **56** No. 3-4 (2005), 64–70.

[18] KAZMIERKOWSKI, M. P.—MALESANI, L.: Current Control Techniques for Three-Phase Voltage-Source PWM Converters: A Survey, IEEE Trans. on Industrial Electronics **45** No. 5 (Oct 1998), 691–703.

[19] HOLTZ, J.: Pulsewidth Modulation — A Survey, IEEE Trans. on Industrial Electronics **39** No. 5 (Dec 1992), 410–420.

[20] MAO, H.—YANG, X.—CHEN, Z.—WANG, Z.: A Hysteresis Current Controller for Single-Phase Three-Level Voltage Source Inverters, IEEE Trans. on Power Electronics **27** No. 7 (July 2012), 3330–3339.

[21] DEY, A.—RAJEEVAN, P.—RAMCHAND, R.—MATHEW, K.—GOPAKUMAR, K.: A Space-Vector-Based Hysteresis Current Controller for a General n-Level Inverter-Fed Drive with Nearly Constant Switching Frequency Control, IEEE Trans. on Industrial Electronics **60** No. 5 (May 2013), 1989–1998.

[22] KENNEL, R.—El-KHOLY, E.—MAHMOUD, S.—El-REFAEI, A.—ELKADY, F.: A Simple High Performance Current Control Scheme for Induction Motor Drives, 31st Annual Conference of IEEE Industrial Electronic Society (IECON), 2005, pp. 1762–1767.

[23] DANDIL, B.—TUNCER, S.: Four Quadrant Control of Multilevel Inverter Fed Induction Motor Drives, Journal of Scientific and Industrial Research **67** (Sep 2008), 688–696.

[24] BOSE, B. K.: Modern Power Electronics and AC Drives, Prentice Hall Inc, New Jersey, 2002.

Received 20 April 2016

Cosmas Ogbuka (Engr Dr) was born in Umuna Nigeria on 1st April, 1981. He received his BEng (First Class Honors), MEng (Distinction) and Doctor of Philosopy PhD in 2004, 2009 and December 2014 respectively in the Department of Electrical Engineering University of Nigeria, Nsukka, where he presently works as a Lecturer I. His research interests are in adjustable speed drives of electrical machines: (DC and AC electric machine torque/speed control with converters and inverters), Electric machines and power electronics. He has published both locally and internationally and attended conferences within Nigeria and abroad. He is a member of Nigerian Society of Engineers (NSE), Nigerian Institution of Electrical Engineers (NIEEE), International Association of Engineers (IAENG) and is registered by the Council for the Regulation of Engineering in Nigeria (COREN). He is presently (Nov. 2015 to April 2016) on a postdoctoral research visit at the Chair of Electrical Drives and Actuators (EAA) Universität der Bundeswehr München, Germany with Professor Dr.-Ing. Dieter Gerling.

Cajethan Nwosu (Engr Dr) was born on 1st October 1967. He obtained the BEng, MEng, and PhD degrees in electrical engineering from the University of Nigeria, Nsukka in 1994, 2004, and 2015 respectively. In 2007, he undertook a three months pre-doctoral research on wind/solar hybrid power system and renewable energy resources at the University of Technology, Delft (TU-Delft), the Netherlands. Since 2005, he has been with the Department of Electrical Engineering, University of Nigeria, Nsukka, where he is currently a senior lecturer. He had written two books and had published over thirty articles both in local and international journals. He is an executive member of Nigerian Institution of Electrical and Electronic Engineers (NIEEE), Nsukka chapter. He is a member of Power Electronics Society of Institution of Electrical and Electronic Engineering (PES IEEE). He is an editorial board member World Science Journal of Engineering Applications. His areas of research interest include power electronic converters, electrical drives and renewable energy technologies.

Marcel Agu (Engr Prof), born on 13th May 1947 in Ohebe-Dim Nigeria, obtained his BSc in electrical engineering in 1974 in the University of Nigeria, Nsukka. He also received his MASc and PhD in 1978 and 1982 respectively in power electronics from the University of Toronto Canada. He is a professor of power electronic in the Department of Electrical Engineering University of Nigeria, Nsukka. His research interests are, but not limited to, power electronic circuits (solid state AC/DC and DC/DC converters, inverter circuits and cycloconverter/inverter circuits), static electric motor drives (DC and AC electric machine torque/speed control with converters and inverters), Analogue, digital and microprocessor-based electronic control circuits, static induction heating power supplies for heat treatment of metals (melting, casting, forging, forming, annealing, hardening), renewable energy sources (especially in the area of working with solar photo voltaic cells and panels to realize solar lighting, heating, battery charging and water pumping), power system distribution for residential, commercial and industrial areas. He has published wide both in local and international journals.